



Measurement of ethylene in combustion exhaust using a 3.3- μm distributed feedback interband cascade laser with wavelength modulation spectroscopy

Kotaro Tanaka¹ · Kazushi Akishima² · Masahiro Sekita² · Kenichi Tonokura³ · Mitsuru Konno¹

Received: 29 January 2017 / Accepted: 17 July 2017 / Published online: 26 July 2017
© Springer-Verlag GmbH Germany 2017

Abstract A sensor for the detection of ethylene (C_2H_4) in combustion exhaust based on a mid-infrared wavelength modulation spectroscopic technique was constructed using a distributed feedback interband cascade laser (DFB-ICL) with a wavelength of 3.3 μm . The direct absorption spectrum of C_2H_4 in the range of 2978.8–2982.1 cm^{-1} was recorded, where the spectrum was in good agreement with the spectrum simulated using parameters from the HITRAN 2012 database. The absorption line at 2979.581 cm^{-1} [$2.42 \times 10^{-21} \text{cm}^2 \text{mol}^{-1} \text{cm}^{-1}$, ν_{11} , $^3\text{P}_5(5)$] was selected for C_2H_4 detection. This frequency was chosen to minimize spectral interference from other major combustion products in the emission frequency range of the DFB-ICL. A limit of detection for C_2H_4 of 96 parts per billion by volume was achieved at a signal-to-noise ratio of two under 3 kPa of pressure using $2f$ wavelength modulation spectroscopy. Using the developed sensor, the ethylene concentration in the exhaust from a portable power generator was also successfully determined.

1 Introduction

Ethylene (C_2H_4) detection is useful in many fields such as combustion chemistry [1, 2], atmospheric chemistry [1], medical diagnostics [3], and biology [1, 4]. In the field of combustion chemistry, C_2H_4 is an important intermediate product formed during hydrocarbon oxidation; thus, the mechanism of hydrocarbon combustion has been investigated using the concentration profiles of C_2H_4 in hydrocarbon oxidation [5]. The typical concentration of C_2H_4 in combustion emission is 1–50 parts per million (ppm); thus, systems for the detection of C_2H_4 require ppm-level sensitivity [6]. In atmospheric chemistry, C_2H_4 is emitted from automobiles and industries, and is a main pollutant that promotes the formation of tropospheric ozone in urban areas [7]. The average concentration of C_2H_4 in air is less than 20 parts per billion (ppb); thus detection systems for such applications require ppb-level sensitivity [8]. In medical research, the concentration of C_2H_4 in breath is measured for renal failure screening [3]. In the field of biology, C_2H_4 is recognized to have a strong influence on the growth and ripening of fruits; thus, it is necessary to control the C_2H_4 concentration level during fruit transportation [4], which requires a system for continuous measurement of the C_2H_4 concentration.

Laser absorption spectroscopy is an effective technique for the detection of trace gases because of its high-sensitivity, fast time resolution, and low cost. Some techniques such as cavity ring down spectroscopy (CRDS), photoacoustic spectroscopy (PAS), and direct absorption spectroscopy coupled with a multi-pass cell were applied to the detection of C_2H_4 [8–20]. In the near-infrared region, C_2H_4 was detected using CRDS, where a detection limit at the ppb-level was achieved [8, 9]. In the mid-infrared region, high-sensitivity measurements of C_2H_4 using a carbon

This article is part of the topical collection “Field Laser Applications in Industry and Research” guest edited by Francesco D’Amato, Erik Kerstel, and Alan Fried.

✉ Kotaro Tanaka
kotaro.tanaka.comb@vc.ibaraki.ac.jp

¹ Department of Mechanical Engineering, Ibaraki University, 4-12-1 Nakanarusawa, Hitachi, Ibaraki 316-8511, Japan

² Graduate School of Science and Engineering, Ibaraki University, 4-12-1 Nakanarusawa, Hitachi, Ibaraki 316-8511, Japan

³ Graduate School of Frontier Sciences, The University of Tokyo, 5-1-5 Kashiwanoha, Kashiwa, Chiba 277-8563, Japan

dioxide gas laser were performed [5, 10–17]. Murtz et al. [10] developed a C_2H_4 sensor using cavity leak-out spectroscopy to achieve a detection limit of 1 ppb. C_2H_4 detection using PAS was also performed and a detection limit of 16 ppb was achieved [11]. A C_2H_4 sensor based on PAS was applied to various studies such as breath analysis [12], flood research [13], investigation of atmospheric C_2H_4 sources [14], and ripening of fruits [15]. Quartz-enhanced PAS with a carbon dioxide gas laser was also applied to the detection of C_2H_4 , where a detection limit of 50 ppb was achieved [16]. Recently, a C_2H_4 detection technique using a carbon dioxide gas laser was also employed for combustion diagnostics by monitoring C_2H_4 during hydrocarbon oxidation [5, 17].

Although the carbon dioxide gas laser has been extensively used for C_2H_4 detection, recently, compact and stable quantum cascade lasers (QCL) with a wavelength range of 4–13 μm were developed and applied to C_2H_4 detection [18–20]. A pulsed QCL at 10.5 μm coupled with a 100 m optical path-length astigmatic Herriott cell was utilized for C_2H_4 detection, where a detection limit of 30 ppb was achieved [18]. A direct absorption spectrometer with a pulsed QCL at 10.26 μm and 66 m optical path-length Herriott cell was also developed and applied to measurement of C_2H_4 and carbon dioxide in automobile exhaust [19]. A 150 m optical path-length astigmatic Herriott cell with a pulsed QCL at 10.3 μm was also used for C_2H_4 and ammonia detection [20].

C_2H_4 shows the strongest absorption peak near 10.5 μm and another strong absorption peak is present in the 3.3 μm region, which is assigned to the ν_{11} fundamental band; C_2H_4 was detected using quartz-enhanced PAS with a distributed feedback laser at 3.32 μm [21]. Recently, a distributed feedback interband cascade laser (DFB-ICL) with a wavelength range of 3–4 μm was developed and applied to trace-gas detection, especially hydrocarbons [22, 23]. The 3 μm region is important for high-sensitivity measurements of hydrocarbons in combustion emission because there are many hydrocarbon absorption bands in the 3 μm region [24]. However, only a few studies have focused on detection of hydrocarbon at trace levels using the DFB-ICL in the 3 μm region.

In this study, a high-sensitivity sensor for the detection of C_2H_4 in combustion exhaust in the 3.3 μm region, based on wavelength modulation spectroscopy (WMS) with a Herriott-type multi-pass cell and a DFB-ICL, is developed. To the best of our knowledge, there are no previous studies on C_2H_4 detection using wavelength modulation spectroscopy with DFB-ICL at 3.3 μm . The optical setup used in this experiment is almost the same as that used in Ref [22], where formaldehyde (HCHO) was detected, except the optical cell. As HCHO also has absorption lines in this

wavelength region [22], an appropriate absorption line of C_2H_4 that does not suffer from interference from HCHO and main combustion emissions such as those of carbon dioxide and water is selected. C_2H_4 in power generator exhaust is also assayed using the developed system.

2 Experiments

2.1 MID-IR laser absorption spectrometer for ethylene measurements

The experimental apparatus at Ibaraki University has previously been described in detail by Tanaka et al. [22], which is shown in Fig. 1. A 3.356 μm DFB-ICL (Nanoplus, Gerbrunn, Germany) with a maximum output power of 1.2 mW was used as the light source. The injection current and the laser-chip temperature of the diode laser were maintained using a laser control unit (ILX LDC3724C, ILX Lightwave, Bozeman, MT, USA). The beam was collimated with an anti-reflection coated aspheric lens ($f = 11$ mm) and introduced into the Herriott-type multi-pass cell (CMP-30, Photonics Technologies, UK). The cell had a path-length of 29.9 m and a volume of 0.9 L. Before introduction into the cell, the beam was focused onto the center of the multi-pass cell using a CaF_2 lens with a focal length of 500 mm. The beam was passed through the multi-pass cell and was focused on an InSb photodiode detector (HAMAMATSU P4631-03, Hamamatsu, Japan).

C_2H_4 was detected using a second-harmonic ($2f$) WMS. The wavelength of the DFB-ICL was modulated sinusoidally at 12.2 kHz using the output of a digital lock-in amplifier (Stanford Research Systems, SR810, Sunnyvale, CA, USA). The laser was scanned at 1 Hz by changing the injection current, which was controlled by a triangle voltage wave supplied by a function generator (Wavestation 2012, Teledyne Lecroy, Chestnut Ridge, NY, USA). The signal obtained from the photo-detector was received by a lock-in amplifier with a 10 ms time constant and 24 dB/oct digital filtering, which corresponded to an equivalent noise bandwidth of 7.8125 Hz. The modulation condition was adjusted to obtain the highest signal-to-noise ratio for the $2f$ WMS of C_2H_4 . The data were acquired using a laptop computer with a 16 bit NI-DAQ system (USB-6216 BNC, National Instruments, Texas, USA).

The multi-pass cell was evacuated using a rotary pump, and the pressure in the cell was monitored using a capacitance manometer (Model 730, Setra, Boxborough, MA, USA). The pressure was kept at 3 ± 0.01 kPa. A PID controller (E5CN-RQ2BT, Omron, Kyoto, Japan) was used to control the gas and cell temperature at 393 ± 0.01 K;

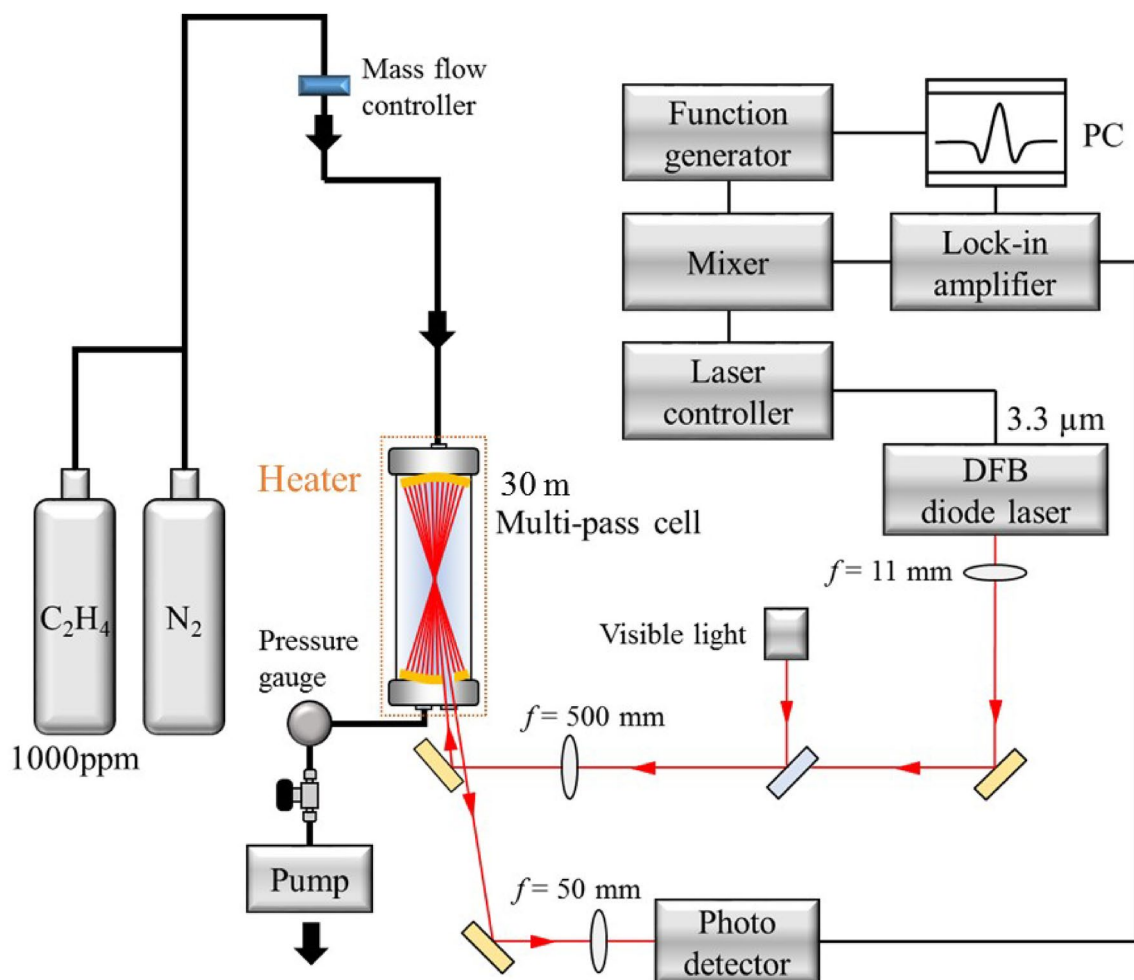


Fig. 1 Schematic diagram of the experimental setup for C_2H_4 sensor optics

998 ppm C_2H_4 gas (Taiyo Nippon Sanso Corp., Japan) diluted with nitrogen, and nitrogen (Taiyo Nippon Sanso Corp., >99.999%) were used as the standard gases.

2.2 Engine exhaust measurement system

A schematic of the sample exhaust system is shown in Fig. 2. A power generator with a gasoline engine was selected as an example of a combustion emission source. To sample the exhaust, a stainless tube was connected to the exhaust pipe of the power generator. The exhaust was introduced into the spectrometer for measuring ethylene at a constant flow rate of 2 standard L min^{-1} , which was controlled by a mass flow controller (Kofloc, 3660 series, Japan). The cell pressure and temperature were set to 3 kPa and 393 K, respectively. The temperature of the sample lines was set to 393 K to avoid water condensation. The operating conditions for the power generator were set to the conditions where the rated power output was obtained.

3 Results and discussion

3.1 Measurements of C_2H_4 spectrum in the 3.3 μm region

A direct absorption spectrum of 998 ppm C_2H_4 diluted with nitrogen (99.999%) was obtained using the experimental setup at a total pressure of 3 kPa in the 2978.8–2982.1 cm^{-1} region, as shown in Fig. 3a. The simulated spectrum is shown in Fig. 3a which was calculated using the parameters in the HITRAN 2012 database [25] at 3 kPa and 393 K. The residuals of the absorbance between the experiments and simulations are also shown in Fig. 3b. The measured spectrum is in good agreement with the simulated one. At around 2981.3 cm^{-1} , there are some residuals between the experiments and simulations. These residuals may be derived from the error of the peak positions obtained from the experiments. A 2f-WMS spectrum of 100 ppm C_2H_4 was also obtained at 3 kPa and 393 K, as shown in Fig. 3c. Although the positions of the WMS

Fig. 2 Schematic diagram of engine exhaust measurement system

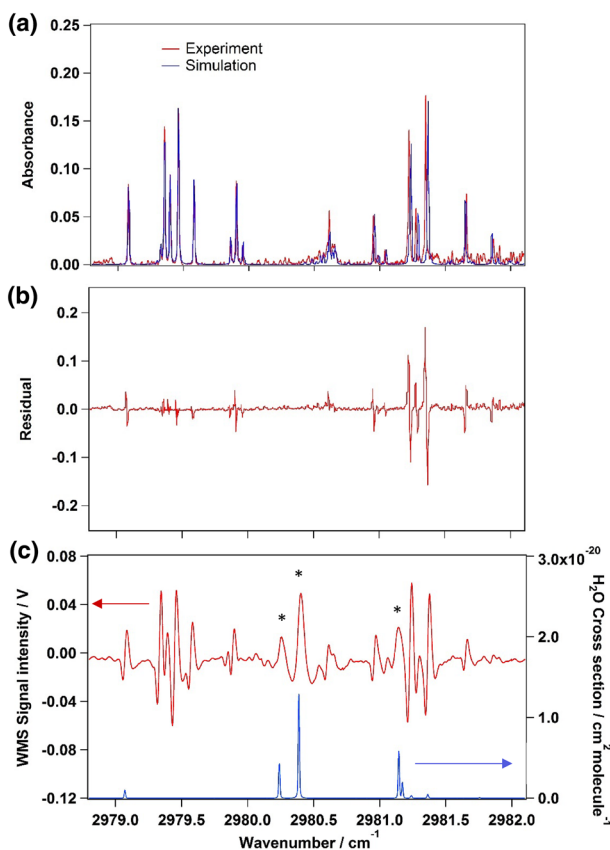
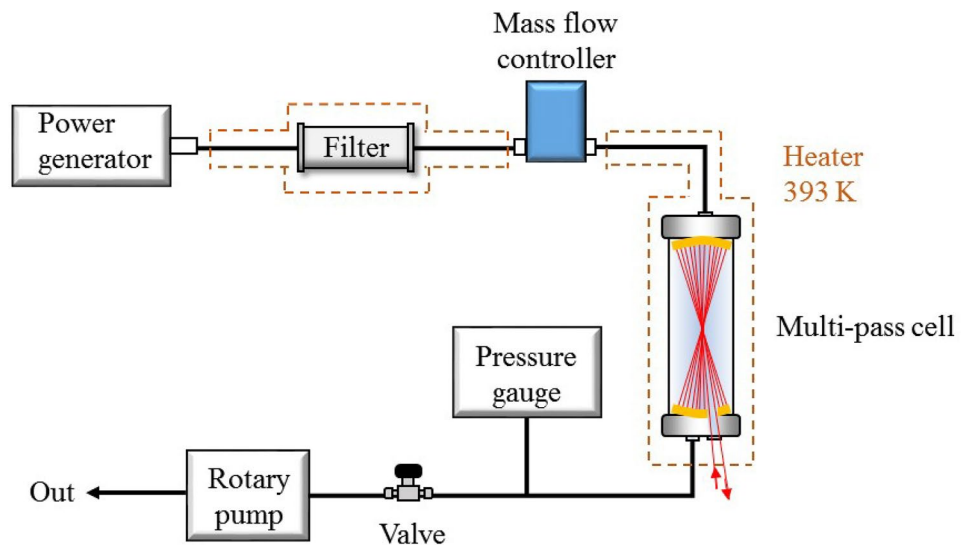


Fig. 3 **a** Experimental and simulated direct absorption spectrum of 998 ppm C_2H_4 at 3 kPa at 393 K. Simulation was performed using spectroscopic parameters in the HITRAN 2012 database [25]; **b** residuals between the experimental spectrum and the simulated one; and **c** second-harmonic WMS signals for 100 ppm C_2H_4 at 3 kPa and 393 K (red trace in the (c) which is referenced to the left axis) and simulated spectrum of water at 3 kPa and 393 K using spectroscopic parameters in the HITRAN 2012 database [25] (blue trace in the (c) which is referenced to the right axis). The absorption peaks labeled by asterisks in (c) correspond to water

peaks were also in good agreement with the simulated spectrum shown in Fig. 3a, WMS peaks that did not appear in the direct absorption spectrum of C_2H_4 were observed, as labeled with asterisks in Fig. 3c. The positions of these peaks are in good agreement with those of water, the cross section of which was calculated using the parameters in the HITRAN 2012 database [25] at 3 kPa and 393 K (Fig. 3c). It is thought that atmospheric water was detected as the laser light passed through the air between the laser source and the cell. Based on the cross section of water at 100 kPa and 298 K ($7.92 \times 10^{-22} \text{ cm}^2 \text{ mol}^{-1}$ at 2980.388 cm^{-1}), water concentration of 1% at experimental room (298 K, 35% of relative humidity), and absorption length of 60 cm between the laser source and the cell, absorbance of water is estimated to be approximately 0.014, which is the same order as those of 100 ppm C_2H_4 derived from the absorbance of 998 ppm C_2H_4 , as shown in Fig. 3a.

An appropriate absorption peak had to be selected for the C_2H_4 analysis during combustion emission because many species are present in combustion emission. The main constituents of combustion emissions are carbon dioxide and water. Carbon dioxide does not possess any absorption peaks in this wavenumber region, whereas water has absorption peaks in this wavenumber region, as shown in Fig. 3c. In addition to water and C_2H_4 , two other species in combustion emission absorb in the wavenumber region of interest; these are HCHO and methane (CH_4). The simulated spectra of the four species, C_2H_4 , HCHO, CH_4 and water, at 3 kPa and 393 K are shown in Fig. 4. In addition, the simulated spectrum of ethane (C_2H_6) at 3 kPa, 296 K is also shown in Fig. 4 [26]. As line parameters of C_2H_6 were obtained under the conditions where the temperature was less than 296 K, the C_2H_6 spectrum was simulated at 296 K instead of 393 K. C_2H_6 has strong absorption peaks in this wavenumber region. However, as the concentration of C_2H_6

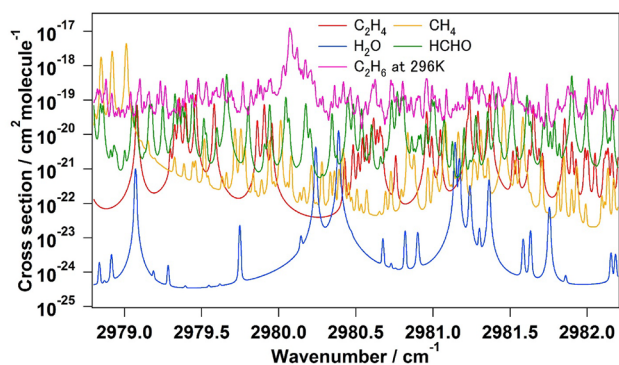


Fig. 4 Simulated spectra of C_2H_4 , HCHO, CH_4 , and water at 3 kPa and 393 K, and simulated spectrum of C_2H_6 at 3 kPa and 296 K

in combustion emission is typically one order less than that of C_2H_4 [27], C_2H_6 has little influence on the measurements of C_2H_4 , which will be discussed in the following Sect. 3.3. Hence, adequate absorption peaks for measurements of C_2H_4 in combustion emission was selected without considering the C_2H_6 absorption peaks.

Based on the simulated data except that of C_2H_6 , the absorption peak of C_2H_4 that does not suffer from interference from HCHO, CH_4 , and water is the absorption line at 2979.581 cm^{-1} [$2.42 \times 10^{-21}\text{ cm}^2\text{ mol}^{-1}\text{ cm}^{-1}$, ν_{11} , $^{\text{P}}\text{P}_5(5)$], which was selected for further analyses. As the weak absorption line of HCHO next to the selected C_2H_4 absorption line may influence quantitative analysis of C_2H_4 , error analysis was performed. The concentrations of HCHO and C_2H_4 are assumed to be 100 ppm. HCHO concentration is almost maximum concentration in typical combustion emission such as automobile exhaust [28]. Absorbance of C_2H_4 was calculated with or without HCHO and peak absorbance of C_2H_4 without HCHO was compared to that with HCHO. The error in the C_2H_4 measurements derived from the interference from the weak HCHO absorption line is estimated to be 15% at a total pressure of 10 kPa and less than 3% at a total pressure of less than 3 kPa. Therefore, the maximum total pressure for analysis of C_2H_4 in combustion emission at $3.356\text{ }\mu\text{m}$ should be less than 3 kPa.

It has also been reported that various kinds of hydrocarbons are present in combustion emission [27–29] and the main species are small hydrocarbons such as C_2H_4 , CH_4 , and HCHO, the concentrations of which are at least twice as high as those of other hydrocarbons [29]. Therefore, even though there is interference from the absorption lines of other hydrocarbons, it is considered that these peaks have little influence on the measurements of C_2H_4 in combustion emission.

Based on the above discussion, the absorption line at 2979.581 cm^{-1} ($2.42 \times 10^{-21}\text{ cm}^2\text{ mol}^{-1}\text{ cm}^{-1}$, ν_{11} , $^{\text{P}}\text{P}_5(5)$)

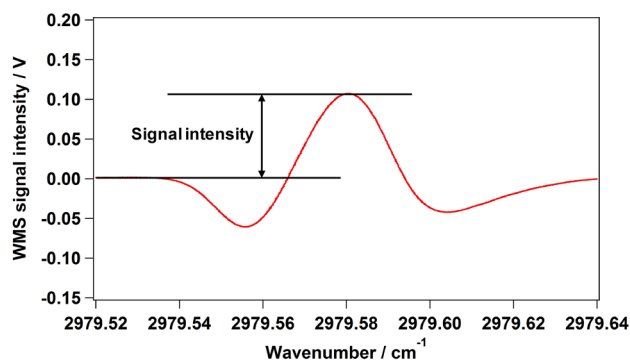


Fig. 5 Second-harmonic WMS signals for 75 ppm C_2H_4 at 2979.581 cm^{-1} at 3 kPa and 393 K

was selected for measurements of C_2H_4 in combustion emission, and the optimal pressure for the measurement was determined to be 3 kPa.

3.2 Limit of detection

The $2f$ WMS spectrum for 75 ppm C_2H_4 at 3 kPa and 393 K is shown in Fig. 5. The signals were averaged over 40 consecutive scans at 1 Hz. The modulation amplitude, $\nu_m/\nu_{\text{C}_2\text{H}_4}$, was optimized to 2.13 to obtain the best signal-to-noise ratio for the $2f$ WMS signal. This modulation amplitude was consistent with the theoretical value of 2.2 [30]. To evaluate the signal stability for the measurement system, continuous measurements of 75 ppm C_2H_4 at 3 kPa and 393 K were performed using $2f$ WMS over 13,000 s. The signal was obtained with 1 Hz resolution. The time series of the C_2H_4 signals and the associated Allan-Werle variance (σ_A^2) are plotted in Fig. 6 [31]. From the Allan-Werle variance plot, an optimum integration time of 40 s with $\sigma_A^2 = 2.21 \times 10^{-8}$ was derived.

The limit of detection was obtained using the signal intensity and the noise level of the spectrum in Fig. 5. The WMS signal intensity was defined as the difference between the peak intensity and the baseline, as shown in Fig. 5. The signal-to-noise ratio of the WMS spectrum for 75 ppm C_2H_4 shown in Fig. 5 was approximately 1530, and the limit of detection for achieving a signal-to-noise ratio of two was 96 ± 6 ppb. A calibration plot of the WMS signal is shown in Fig. 7. The signal intensity was proportional to the C_2H_4 concentrations. The slope and the noise level, which was determined from the average baseline deviation, were used to calculate the limit of detection for a signal-to-noise ratio of two. The limit of detection was 96 ± 4 ppb, which is in good agreement with the limit of detection mentioned above.

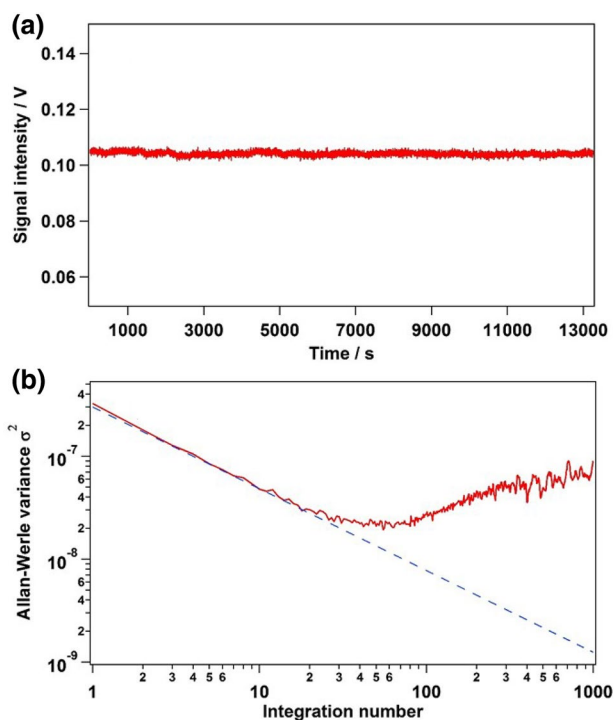


Fig. 6 **a** Time profiles of the 75 ppm C_2H_4 signals at 3 kPa and 393 K; **b** Allan-Werle variance plot. The *blue dashed* line indicates white noise

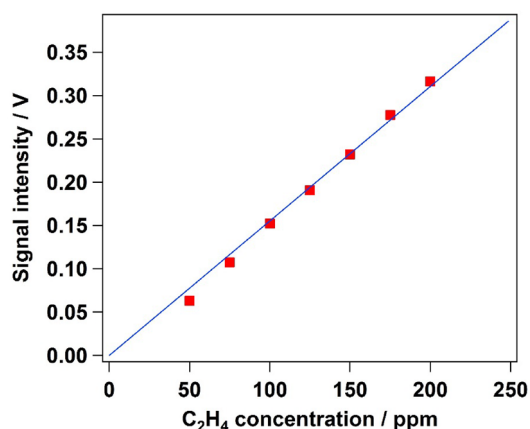


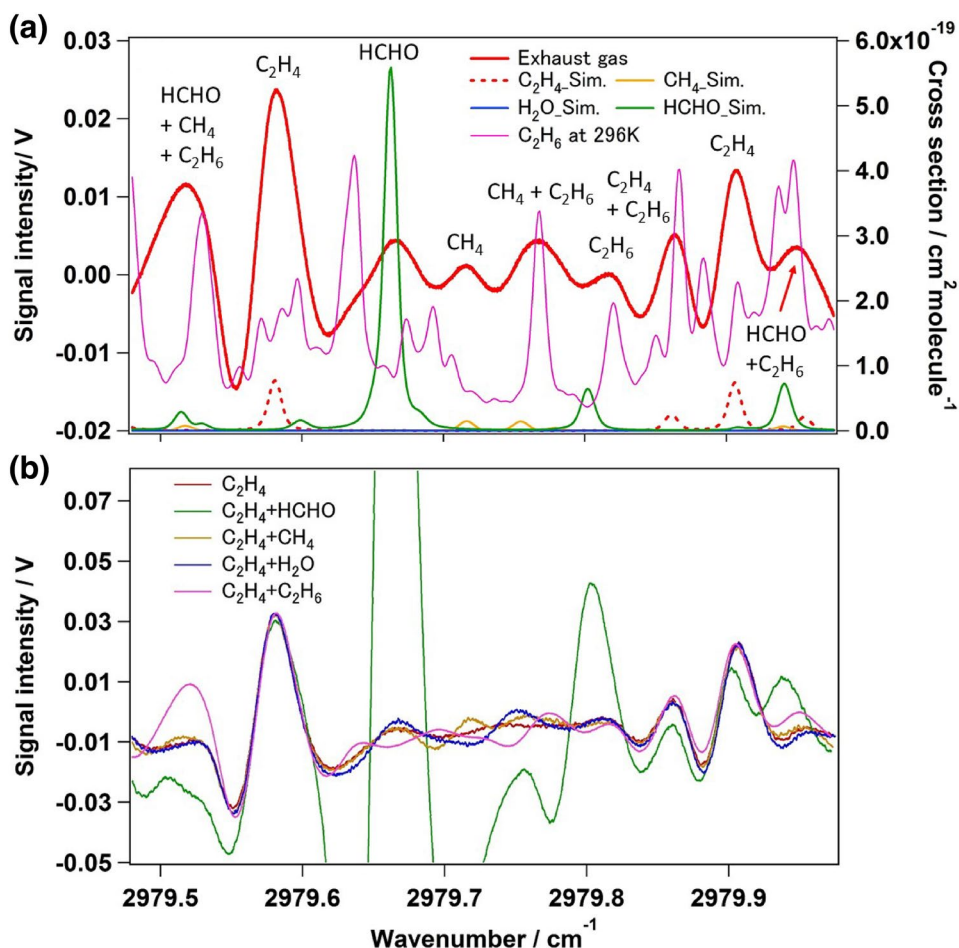
Fig. 7 Signal intensity of C_2H_4 as a function of concentration. A least squares fitting line is also shown in the graph

3.3 C_2H_4 measurements in combustion emission

The C_2H_4 in combustion emission was measured using a WMS measurement system to illustrate the potential of the system. The combustion emission from a portable power generator was introduced into the cell after the engine was stabilized. The spectrum of the exhaust is shown in Fig. 8a. Reference spectra of 100 ppm C_2H_4 ,

a mixture of 100 ppm C_2H_4 and 100 ppm HCHO, a mixture of 100 ppm C_2H_4 and 100 ppm CH_4 , a mixture of 100 ppm C_2H_4 and 1% water, and a mixture of 100 ppm C_2H_4 and 10 ppm C_2H_6 are also shown in Fig. 8b, which were obtained under the same conditions as those where the spectrum of the exhaust was obtained. The simulated spectra of C_2H_4 , HCHO, CH_4 , and water at 3 kPa and 393 K, and the simulated spectrum of C_2H_6 at 3 kPa and 296 K are shown in Fig. 8a. Signals at the wavenumber of the C_2H_4 absorption peak in the exhaust spectrum were observed, whose peak positions were in good agreement with those of reference spectrum of C_2H_4 and the simulated spectrum. The spectrum of the exhaust in Fig. 8a shows absorption peaks of certain species. Based on the reference spectra and the simulated spectrum, HCHO, CH_4 , and C_2H_6 had absorption peaks in the wavenumber region used for the present C_2H_4 measurement. When the HCHO was included in the reference gas mixture, the C_2H_4 signal intensity at 2979.581 cm^{-1} was changed slightly compared to that without HCHO. The error derived from this difference was less than 3% that mentioned in above sections. The weak peak of HCHO (2979.599 cm^{-1}) next to the selected C_2H_4 absorption peak (2979.581 cm^{-1}) could not measure the reference spectrum. Although water had extremely small absorption peaks between 2979.0 and 2980.0 cm^{-1} , whose order of integrated cross section is 10^{-27} – $10^{-29}\text{ cm}^2\text{ mol}^{-1}\text{ cm}^{-1}$, water that had typical concentration in the combustion emission (5–15%) had no influence on the C_2H_4 measurements in this wavenumber region. As C_2H_6 has the absorption peaks in this wavenumber region, the reference spectrum of mixture of 100 ppm C_2H_4 with 10 ppm C_2H_6 were obtained, whose concentration is typical in the combustion emission [27]. Although the signal intensity of the selected C_2H_4 absorption peak was slightly changed, the error derived from the interference of C_2H_6 was less than 3%. If the emission level of C_2H_6 is relatively high against the C_2H_4 , C_2H_6 concentration is required to be monitored to obtain the precise C_2H_4 concentration in the exhaust using this instrument. To compare the concentrations obtained by gas chromatography-flame ionization detector (GC-FID) to those obtained by the developed instrument, the concentrations of C_2H_6 and C_2H_4 in the exhaust emitted from the portable power generation system were measured using GC-FID, and found to be 2.3 and 23 ppm, respectively, which was the same tendency as those of typical combustion emission [27]. Hence, C_2H_6 had little influence on the measurements of C_2H_4 in the combustion emission. The obtained signal intensities were calibrated using the signals of C_2H_4 standard gas, and the C_2H_4 concentration was estimated to be $28 \pm 5\text{ ppm}$, which is in agreement with the concentration of C_2H_4 measured using GC-FID. These results

Fig. 8 a Combustion emission spectrum in the 2979.48–2979.97 cm^{-1} region with averaging over 40 consecutive scans at 1 Hz. The cell temperature and pressure were 393 K and 3 kPa, respectively. Simulated spectra of C_2H_4 , water, HCHO, and CH_4 at 393 K and 3 kPa, and the simulated spectrum of C_2H_6 at 296 K and 3 kPa are also shown in this graph; **b** reference spectra of 100 ppm C_2H_4 , a mixture of 100 ppm C_2H_4 and 100 ppm HCHO, a mixture of 100 ppm C_2H_4 and 100 ppm CH_4 , a mixture of 100 ppm C_2H_4 and 1% water, and a mixture of 100 ppm C_2H_4 and 10 ppm C_2H_6 measured under the same conditions where the combustion emission spectrum is obtained



demonstrate that the C_2H_4 measurement system based on WMS has powerful potential for the detection of trace gaseous C_2H_4 in combustion emission.

4 Conclusion

A sensitive spectrometer was constructed for trace gas analysis of C_2H_4 in combustion emission using WMS coupled with a Herriott-type multi-pass cell and a DFB-ICL at 3.356 μm . To minimize spectral interference from major combustion products in the emission frequency range of the DFB-ICL, the C_2H_4 absorption line at 2979.581 cm^{-1} ($2.42 \times 10^{-21} \text{ cm}^2 \text{ mol}^{-1} \text{ cm}^{-1}$, ν_{11} , $^3\text{P}_5(5)$) was selected for analysis of C_2H_4 in combustion emission and the optimal maximum total pressure in the cell was determined to be less than 3 kPa. The estimated limit of detection was 96 ± 6 ppb at 393 K and 3 kPa, where the signal was averaged over 40 consecutive scans. Analysis of C_2H_4 in combustion emission was successfully performed with the developed system. These results indicate that this measurement system is a potentially powerful tool for measurement

of trace gaseous C_2H_4 in combustion emissions, such as in automobile exhaust.

Acknowledgements The authors thank an anonymous reviewer to inform C_2H_6 absorption spectra. This study was partly supported by JSPS KAKENHI (Grant Numbers 16K18023 and 26288086) and by the Council for Science, Technology, and Innovation (CSTI), Cross-ministerial Strategic Innovation Promotion Program (SIP), “Innovative Combustion Technology” (Funding agency: JST).

References

1. D.A. Morgott, Chem. Biol. Interact. **241**, 10 (2015)
2. M.J. Pilling, *Low-Temperature Combustion and Autoignition: Comprehensive Chemical Kinetics* (Elsevier, Amsterdam, 1997)
3. C. Popa, M. Patachia, S. Banita, C. Matei, A. Bratu, D. Dumitras, Laser Phys. **23**(10), 125701 (2013)
4. S. Janssen, K. Shmitt, M. Blanke, M.L. Bauersfeld, J. Wollenstein, W. Lang, Math. Phys. Eng. Sci. **372**(2017), 20130311 (2014)
5. M.B. Sajid, T. Javed, A. Farooq, Comb. Flame **164**, 1 (2016)
6. C.G. Teodoro, D.U. Schramm, M.S. Stel, G.R. Lima, M.V. Rocha, J.R. Tavares, H. Vargas, Infrared Phys. Technol. **53**, 151 (2010)
7. J.H. Seinfeld, Science **243**(4892), 745 (1989)

8. M.S. Aziz, A.J. Orr-Ewing, J. Environ. Monit. **14**(12), 3094 (2012)
9. E. Wahl, S. Tan, S. Koulikov, B. Kharlamov, C. Rella, E. Crosson, D. Biswell, B. Paldus, Opt. Express **14**(4), 1673 (2006)
10. M. Murtz, B. Frech, W. Urban, Appl. Phys. B **68**(2), 243 (1999)
11. G. Mothe, M. Castro, M. Sthel, G. Lima, L. Brasil, L. Campos, A. Rocha, H. Vargas, Sensors **10**(11), 9726 (2010)
12. F.J.M. Harren, R. Berkelmans, K. Kuiper, S. Hekkert, P. Scheepers, R. Dekhuijzen, P. Hollander, D.H. Parker, Appl. Phys. Lett. **74**(12), 1761 (1999)
13. L. Voesenek, M. Banga, J. Rijnders, E. Visser, F. Harren, R. Brailsford, M. Jackson, C. Bolm, Ann. Bot. **79**, 57 (1997)
14. J.A. de Gouw, S. te Lintel Hekkert, J. Mellqvist, C. Warneke, E.L. Atlas, F.C. Fehsenfeld, A. Fried, G.J. Frost, F.J. Harren, J.S. Holloway, B. Lefer, R. Lueb, J.F. Meagher, D.D. Parrish, M. Patel, L. Pope, D. Richter, C. Rivera, T.B. Ryerson, J. Samuelsen, J. Walega, R.A. Washenfelder, P. Weibring, X. Zhu, Environ. Sci. Technol. **43**(7), 2437 (2009)
15. Y.Y. Leshem, Y. Pinchasov, J. Exp. Bot. **51**(349), 1471 (2000)
16. Z. Wang, Z. Li, W. Ren, Opt. Express **24**(4), 4143 (2016)
17. W. Ren, D.F. Davidson, R.K. Hanson, Int. J. Chem. Kinet. **44**(6), 423 (2012)
18. D. Weidmann, A.A. Kosterev, C. Roller, R.F. Curl, M.P. Fraser, F.K. Tittel, Appl. Opt. **43**(16), 3329 (2004)
19. M.T. McCulloch, N. Langfold, G. Duxbury, Appl. Opt. **44**(14), 2887 (2005)
20. J. Manne, W. Jager, J. Tulip, Appl. Phys. B **94**(2), 337 (2009)
21. T. Nguyen Ba, M. Triki, G. Desbrosses, A. Vicet, Rev. Sci. Instrum. **86**(2), 023111 (2015)
22. K. Tanaka, K. Miyamura, K. Akishima, K. Tonokura, M. Konno, Infrared Phys. Technol. **79**, 1 (2016)
23. C. Li, L. Dong, C. Zheng, F.K. Tittel, Sens. Actuators B Chem. **232**, 188 (2016)
24. R.K. Hanson, D.F. Davidson, Prog. Energy Combust. Sci. **44**, 103 (2014)
25. L.S. Rothman, I.E. Gordon, Y. Babikov, A. Barbe, D.C. Benner, P.F. Bernath, M. Birk, L. Bizzocchi, V. Boudon, L.R. Brown, A. Campargue, K. Chance, E.A. Cohen, L.H. Coudert, V.M. Devi, B.J. Drouin, A. Fayt, J.M. Flaud, R.R. Gamache, J.J. Harrison, J.M. Hartmann, C. Hill, J.T. Hodges, D. Jacquemart, A. Jolly, J. Lamouroux, R.J. Le Roy, G. Li, D.A. Long, O.M. Lyulin, C.J. Mackie, S.T. Massie, S.N. Mikhailenko, H.S.P. Muller, O.V. Naumenko, A.V. Nikitin, J. Orphal, V. Perevalov, A. Perrin, E.R. Polovtseva, C. Richard, M.A.H. Smith, E. Starikova, K. Sung, S. Tashkun, J. Tennyson, G.C. Toon, V.I.G. Tyuterev, G. Wagner, J. Quant. Spectrosc. Radiat. Transf. **130**, 4 (2013)
26. J.J. Harrison, N.D.C. Allen, P.F. Bernath, J. Quant. Spectrosc. Radiat. Transf. **111**, 357 (2010)
27. H. Klingenberg, *Automobile Exhaust Emission Testing* (Springer, Berlin, Heidelberg, 1996)
28. K.F. Ho, S.S.H. Ho, S.C. Lee, P.K.K. Louie, J. Cao, W. Deng, Aerosol. Air Qual. Res. **13**, 1331 (2013)
29. J.Y. Chin, S.A. Batterman, W.F. Northrop, S.V. Bohac, D.N. Assanis, Energy Fuels **26**, 6737 (2012)
30. J. Reid, D. Labrie, Appl. Phys. B **26**, 203 (1981)
31. P. Werle, R. Mucke, F. Slemr, Appl. Phys. B **57**, 131 (1993)